Available online at www.sciencedirect.com
ScienceDirect
Journal of Sound and Vibration 324 (2009) 332–349
JOURNAL OF SOUND AND VIBRATION
www.elsevier.com/locate/jsvi

Liquid sloshing in half-full horizontal elliptical tanks

Seyyed M. Hasheminejad*, Mostafa Aghabeigi

Acoustics Research Laboratory, Department of Mechanical Engineering, Iran University of Science and Technology, Narmak, Tehran 16844, Iran

Received 24 November 2008; received in revised form 18 January 2009; accepted 21 January 2009
Handling Editor: A.V. Metrikine
Available online 3 March 2009

Abstract

A two dimensional hydrodynamic analysis based on the linear potential theory is introduced to study the natural sloshing frequencies of transverse modes in a half-filled non-deformable horizontal cylindrical container of elliptical cross section, without or with a pair of inflexible horizontal longitudinal side baffles of arbitrary extension positioned at the free liquid surface. Successive conformal coordinate transformations in conjunction with the method of separation of variables and the relevant boundary conditions are employed to obtain standard truncated matrix eigen-value problems which are then solved numerically for the resonance eigen-frequencies. The Gauss–Laguerre quadrature formula is used to approximate the integral eigen-problem obtained in the unbaffled case. Plots of the sloshing frequencies as functions of the container aspect ratio and baffle extension are presented and discussed for the three lowest antisymmetric and symmetric transverse oscillation modes. A convergence study is performed to demonstrate the fast convergence and remarkably small computational cost of the Fourier series approach used for the baffled container, and the effects of tank geometry and baffle length on the convergence are also examined. Limiting cases are considered and good agreements with available analytic and numerical solutions as well as experimental data are obtained, demonstrating the accuracy of proposed models.

1. Introduction

Sloshing is a fascinating physical phenomenon characterized by the oscillation of the unrestrained free surface of the liquid in a partially filled container due to external excitation. The understanding of this complex dynamic behavior is of immense practical interest that has far reaching implications encompassing a wide field of technologies and engineering disciplines. Sloshing occurs in moving vehicles with contained liquid masses, such as liquid bulk cargo carriers (e.g., trucks, railroad cars, oil tankers, ships), rockets, aircrafts, and spacecrafts as well as in seismically excited storage tanks, dams, reactors, and nuclear vessels. If the sloshing frequency is sufficiently close to the natural frequency of the structure, resonance can result in instabilities with catastrophic consequences. For example, liquid cargo–vehicle interaction in partly filled tanks has been recognized as a potential contributing factor for the occurrence of about 4% of heavy truck road accidents [1]. In this context, maneuvers performed by the vehicle should not represent even near-to-resonance situations.

*Corresponding author. Tel.: +98 912 7371354; fax: +98 921 77240488.
E-mail address: hashemi@iust.ac.ir (S.M. Hasheminejad).

0022-460X/$ - see front matter © 2009 Elsevier Ltd. All rights reserved.
doi:10.1016/j.jsv.2009.01.040

Similarly, the failure of the spacecraft's control system has been attributed to the destabilizing effects caused by sloshing within liquid stores carried abroad space transportation vehicles [2].

Liquid sloshing in a rigid container has been studied for many years [3]. The problem is generally nonlinear, even if the governing equations of the fluid motion is linearized, in the sense that the free surface boundary condition is nonlinear as well as the position of the free surface is not known *a priori*. In spite of that the complete linearization of the system in which the free surface boundary condition is linearized and satisfied on the undisturbed free surface can give satisfactory results in many cases. There are numerous successful applications of the linearized and nonlinear theories in the open literature. Exhaustive surveys on both formulations can be found in Ref. [3,4]. Just recently, Wei et al. [5] established a finite element method (FEM) for modal and damping analysis of the liquid small amplitude sloshing in containers of arbitrary shape with three kinds of contact line boundary conditions (i.e., free-end, pin-end, and wetting boundary conditions). Liu and Lin [6] developed a numerical two-phase fluid flow model (NEWTANK) to study three-dimensional (3D) highly nonlinear (violent) and turbulent viscous and inviscid liquid sloshing with broken free surfaces in rigid rectangular tanks under arbitrarily six degree-of freedom external excitations. Mitra et al. [7] developed a pressure-based Galerkin finite element code to investigate two-dimensional (2D) slosh characteristics (i.e., natural frequencies, free surface profiles and the hydrodynamic pressure) in partially filled ground-supported containers of various practical shapes (e.g., rectangular, vertically mounted annular cylindrical, trapezoidal and horizontal circular cylindrical containers). Virella et al. [8] used conventional finite element tools (ABAQUS) to investigate the influence of nonlinear wave theory on the 2D sloshing frequencies and their modal pressure distributions for rectangular tanks. The authors examined the effect of the tank geometry and the liquid level, and concluded that the nonlinearity of the surface wave does not have major effects in the pressure distribution on the walls of rectangular tanks. Maleki and Ziyaeifar [9] developed a theoretical damping model based on Laplace's differential equation to investigate the potential of horizontal ring and vertical blade baffles in increasing the hydrodynamic damping of sloshing in circular-cylindrical storage tanks. The authors also carried out a series of experiments employing a tank model on a shake-table to validate their theoretical model. Drosos et al. [10] developed a simple yet accurate numerical methodology based on standard FEM analyses (ANSYS) for effective computation of the eigen-mode frequencies and shapes of the sloshing modes in liquid storage tanks of arbitrary shape and fill height. Attari and Rofooei [11] investigated the lateral nonlinear response of a single degree of freedom (SDOF) structural system containing a rigid circular cylindrical liquid tank. The authors numerically solved for the response under horizontal harmonic and earthquake excitations using the first and third sloshing modes in the neighborhood of 1:2 and 1:1 internal resonances. They found that due to nonlinear interaction between the liquid and the structure, energy transfer from the structure to liquid would take place causing an increase in liquid's response while reducing the response of the structural system.

Horizontal cylindrical tanks with circular cross sections are widely used in road transportation and civil engineering for carrying and storing liquids. Partial fill conditions are quite common during the service time of these tanks. Generally, the analysis of sloshing in horizontal cylindrical vessels filled up to an arbitrary height requires a numerical solution. However, for the particular case of a half-full horizontal cylinder it is possible to develop an analytical solution. Budiansky [12] developed an integral-equation (Green's function) approach to estimate the natural frequencies, (antisymmetric) mode shapes, and forces exerted on the rigid walls of a partially filled 2D circular canal for arbitrary depth of liquid due to lateral excitation by using proper space transformations and quadrature approximations. Using experimental techniques, McCarty and Stephens [13], and Kana [14] measured natural frequencies for transverse sloshing in horizontal cylindrical vessels of different sizes, fullness, and orientations, verifying the results of Budiansky [12]. Moiseev and Petrov [15] described the application of Ritz variational method for the numerical calculation of sloshing frequencies in vessels of various geometries, including the case of a horizontal cylindrical container. Fox and Kuttler [16] used conformal mapping and the powerful method of intermediate problems to obtain upper and lower bounds for the values of 2D sloshing frequencies in a semi-circular tank. The authors also considered regions with baffles, partial lids, double-surfaced sloshers, and a class of more general universal upper-bounding regions. McIver [17] exploited bipolar coordinates to study the 2D sloshing frequencies of fluid in a horizontal circular cylindrical container filled up to an arbitrary height, reformulating the eigen-value-sloshing problem in terms of integral equations, which were then solved numerically. Kobayashi et al. [18], reported

experimental measurements for sloshing frequencies and hydrodynamic forces in horizontal cylinders in both longitudinal and transverse directions under small and large slosh wave heights, and made comparison with analytical values from equivalent rectangular containers. McIver and McIver [19] presented simple analytical methods to obtain upper and lower bounds of sloshing frequencies in horizontal cylinders, which were found to be in good agreement with the results from a boundary element numerical solution. Evans and Linton [20] used nonorthogonal bounded harmonic spatial function expansions to present an accurate series-type semi-analytical solution to the eigenvalue-sloshing problem of half–full horizontal cylindrical containers. Papaspyrou et al. [21,22] used the semi-analytical series-type solution of Evans and Linton [20], to investigate the 2D and 3D sloshing response of half-full rigid horizontal cylindrical vessels under external excitation in the transverse and longitudinal directions. Patkas and Karamanos [23] reported on externally induced sloshing calculations in horizontal cylinders under transverse excitation, using a variational formulation.

Tanks with elliptical cross sections are also extensively used in the road transportation industry. In comparison with the circular case, there are relatively few reports on sloshing studies for this specific configuration in the current literature. Many of these studies are associated with performance of elliptical tank vehicles, and aim to assess directly the stability of the system by identifying the overturning limit or rollover threshold acceleration for different tank shapes and fill levels. For example, Strandberg [24] compared the performance (stability) of circular, elliptical, and super-elliptical tank shapes of equal capacity. He noticed that, for some values of fill level, a circular cross-section tank may be more stable than an elliptical tank of equal capacity. Strandberg concluded that the natural sloshing frequency and the vehicle stability increases in the following order: super-elliptical, elliptical and circular, despite that the centre-of-gravity is also increased in that order. Rakheja et al. [25] investigated the influence of tank size and cross section on the rollover threshold of partially filled articulated tank vehicles during the turning process. The authors carried out computer simulation for steady turning characteristics of a four compartment tank of circular, elliptical, modified oval, and modified square cross sections. Popov et al. [26] presented a numerical analysis of liquid load in elliptical road containers undergoing a uniform lateral acceleration for containers of unrestricted size. They performed an optimization study with an objective to minimize the peak overturning moment on containers of fixed capacity to identify the optimal height–width ratio of the container. Salem [27] simulated the lateral fluid sloshing effects (rollover stability) in partially filled heavy duty elliptical and cylindrical tankers using an equivalent mechanical (trammel) pendulum. He obtained the appropriate pendulum parameters by matching the pendulum dynamic effects with fluid sloshing dynamic effects by using finite element (FE) fluid models. More recently, Xu [28] developed a new mathematical method for investigating 2D and 3D transient liquid motion in partially filled horizontal circular cylindrical and elliptical cargo tanks. The author used continuous coordinate mappings to rearrange the governing equations in such a way that the difficulties of direct discretization for numerical calculation by finite difference method are avoided. Also, Romero et al. [1] described experimental determination of sloshing frequencies based on scale model tests for three tanks with different shapes but equal volume capacities, i.e., two conventional (circular and elliptical) and one generic geometric design. They concluded that, since high natural frequencies are desirable, the elliptical tank is the poorest choice at all fill levels, while the generic tank has the most rapidly increasing natural frequency over the largest range, and has the best performance of all the tanks at high fill levels.

The above review clearly indicates that while there exists a relatively large body of literature on liquid sloshing in horizontal circular cylindrical containers with different fill levels, rigorous analytic or semi-analytic solutions for lateral liquid motion in a half-full horizontal elliptical fluid container (with or without horizontal side baffles) seems to be nonexistent. Our primary objective is to fill this gap. The proposed model is of noble interest essentially due to its inherent value as a canonical problem in liquid sloshing dynamics. It can be of practical value in stability analysis of circular or elliptic cylindrical cargo tanks in near-half-full condition, which are known to be unfavorably connected with the lowest rollover-threshold accelerations [24]. It can serve as an alternative to the numerical (experimental) methods, which may encounter a number of drawbacks such as time-consuming modeling process and numerical computations (excessive measurement noise, non-repeatability of test results, and expensive large-scale laboratory facilities). It may readily be implemented into a computer-aided-design and development chain to guarantee an efficient and optimum design process. Lastly, the presented analytic (semi-analytic) solution can provide a valuable benchmark for comparison to other solutions obtained by strictly numerical or asymptotic approaches.

2. Formulation

2.1. Baffled container

The baffled container geometry is shown in Fig. 1a. An incompressible and non-viscous liquid fills a rigid horizontal elliptic tank, with the major and minor semi-axes "a" and "b," to its half capacity, and two internal horizontal longitudinal side baffles of length "L" partly cover free surface of the fluid as shown in the figure. Such baffles or separators may be used in tank vehicles to impede the lateral slosh and improve rollover stability and performance. The 2D Cartesian coordinates (x, y) are chosen in a plane perpendicular to the cylinder generators. The x axis is in the plane of free surface, which occupies $(L-a)<x<(a-L)$, and y axis points vertically downwards through the midpoint of the free surface. Mathematically, the problem may be stated as follows. The velocity potential for the small time-harmonic irrotational motion (the harmonic time factor is omitted in the following) of the inviscid, incompressible fluid must satisfy Laplace's equation in the fluid domain [3]

$$\nabla^2\Phi(x,y)=0, \tag{1}$$

with the linearized free-surface boundary condition

$$\lambda\Phi+\frac{\partial\Phi}{\partial y}=0, \tag{2}$$

where $\lambda=\omega^2/g$, ω is circular frequency of the oscillations, and g is the acceleration due to gravity. In addition, the zero normal derivative at the rigid wall of the container implies that

$$\frac{\partial\Phi}{\partial n}=0, \tag{3}$$

where n is the normal to the container boundary (see Fig. 1). The above system describes an eigenvalue problem with the eigenvalue λ appearing in the boundary condition (2) rather than the differential equation.

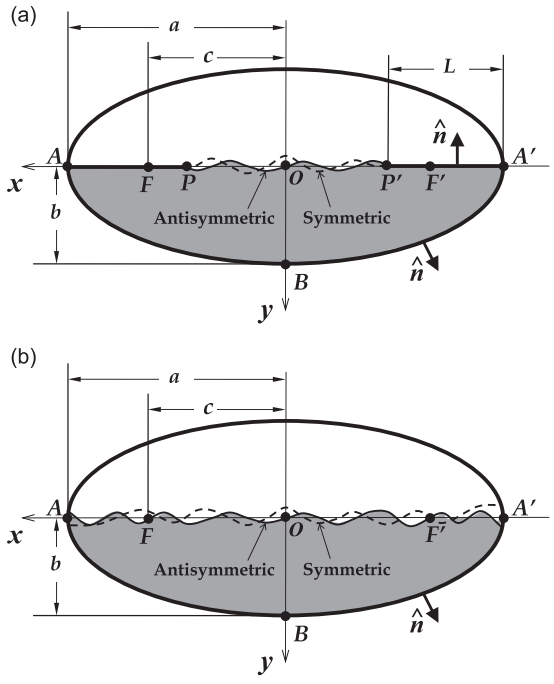

Fig. 1. Problem geometry: (a) baffled elliptical tank and (b) unbaffled elliptical tank.

Since there does not exist a proper choice of the coordinate system for which all coordinate surfaces are wall or free liquid surface, we can use the concept of conformal transformation to relate the original semi-elliptical region to one of the standard regions for which explicit solutions are known such as the rectangle, or the infinite strip. In particular, we manage the exact satisfaction of the boundary conditions at the container wall, side baffles, and the free liquid surface by utilizing appropriate coordinate surfaces. In each case we obtain a Fourier-series expansion for the velocity potential in terms of the transformation variables. The successive transformations shown in the first column of Fig. 2 map the inner region of the half-ellipse with two side baffles, shown Fig. 2a, into a rectangular region in Fig. 2e. Such mapping can be constructed in four steps, as explained below. First, we let R_z denote the half ellipse region of Fig. 2a with distinguished boundary points A, A', B, F, F', P, P' and O. By using the transformation $u=\sin^{-1}(z/c)$; $z=x+iy$, where $c=\sqrt{a^2-b^2}$ is the focal distance of the ellipse, the rectangle R_u of width π and height $\log\rho$, where ρ is defined by $\rho=(a+b)/c$, is obtained (Fig. 2b). Subsequently, following standard notation, R_u is mapped to a half-disk R_v of radius $m_1^{-1/4}$ (Fig. 2c) by the use of Jacobi elliptic sine function $v=\mathrm{sn}[(2K_1u/\pi)|m_1]$, in which $K_1=K(m_1)=\int_0^{\pi/2}(\mathrm{d}\theta/\sqrt{1-m_1\sin^2\theta})$ is the classical elliptic integral of first kind [22,23]. Here, the Jacobi elliptic sine function may be defined as $\mathrm{sn}[\eta|m]=\sin\varphi=\sin[F^{-1}(\eta,m)]$, where $\eta=F(\varphi,m)=\int_0^{\varphi}(\mathrm{d}\theta/\sqrt{1-m\sin^2\theta})$, and φ is known as the Jacobi amplitude [29,30]. Also, given ρ, the parameter $0\leqslant m_1\leqslant 1$ can be calculated by the rapidly convergent series expression [30]

$$m_1^{1/4}=\frac{2\sum_{j=1}^{\infty}\rho^{-4(j-1/2)^2}}{1+2\sum_{j=1}^{\infty}\rho^{-4j^2}}. \tag{4}$$

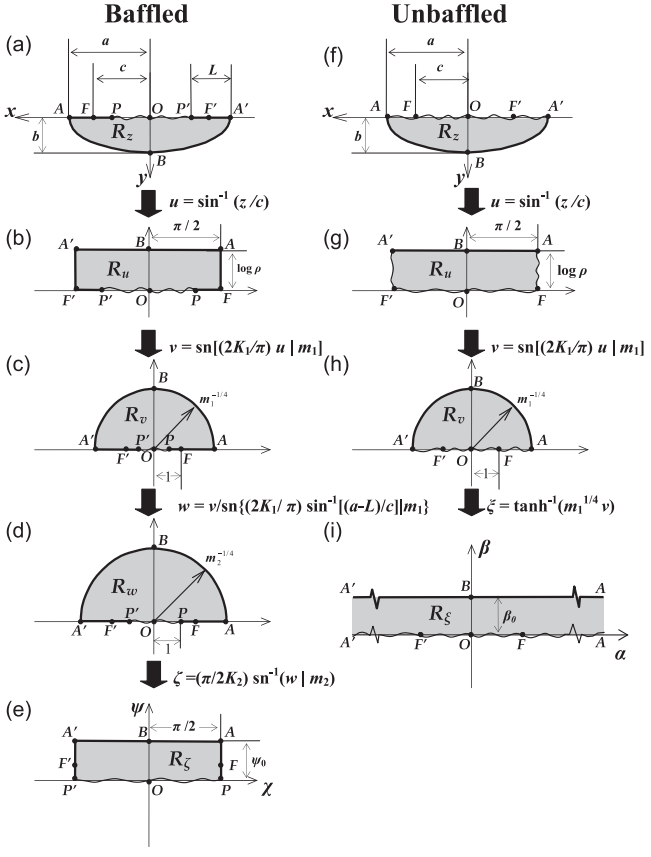

Fig. 2. The successive conformal transformations used for the baffled and unbaffled half-elliptical regions.

Here, we note that corner points F and F' in R_u (Fig. 2b) are mapped into the boundary points (1,0) and (−1,0) in R_v (Fig. 2c), respectively. Next, by the simple scaling, $w = v\{\mathrm{sn}[(2K_1/\pi)\sin^{-1}((a-L)/c)|m_1]\}^{-1}$, the boundary points P and P' are, respectively, mapped into the points (1,0) and (−1,0), and the radius of the new half disk R_w is given by $m_2^{-1/4} = m_1^{-1/4}\{\mathrm{sn}[(2K_1/\pi)\sin^{-1}((L-a)/c)|m_1]\}^{-1}$ (Fig 2d). At this point, we recall the special mapping of corner points F and F' in R_u (Fig. 2b) into the boundary points (± 1,0) in R_v (Fig. 2c). This suggests that the boundary points $P(1,0)$ and $P'(-1,0)$ in R_w (Fig. 2d) may advantageously be mapped into the corner points of a rectangle $(\pm\pi/2, 0)$ through an inverse Jacobi elliptic sine transformation. Consequently, Fig. 2e shows that R_w is mapped into a rectangular region R_ζ by the function $\zeta = (\pi/2K_2)\mathrm{sn}^{-1}[w|m_2]$, where $m_2 = m_1\mathrm{sn}^4[(2K_1/\pi)\sin^{-1}((a-L)/c)|m_1]$, and $K_2 = K(m_2)$ is the classical elliptic integral of the first kind with parameter m_2. Lastly, combining the above steps, one obtains the overall baffled half-ellipse to rectangle map (i.e., R_z in Fig. 2a to R_ζ in Fig. 2e):

$$\zeta = \chi + i\psi = \frac{\pi}{2K_2}\mathrm{sn}^{-1}\left[\frac{\mathrm{sn}[(2K_1/\pi)\sin^{-1}(z/c)|m_1]}{\mathrm{sn}[(2K_1/\pi)\sin^{-1}((a-L)/c)|m_1]}\middle| m_2\right]. \tag{5}$$

It is clear from Fig. 2e that the side baffles are appropriately mapped into the two vertical sides of the rectangle R_ζ, and the y axis coincides with ψ ($\chi = 0$) axis. Also, the elliptical container boundary (liquid free surface) coincides with the coordinate line $\psi = \psi_0(\psi = 0)$.

Now, making use of the change of variables (5), Laplace's equation (1) for the potential $\Phi(\chi,\psi)$ within R_ζ may be written as

$$\frac{\partial^2\Phi}{\partial\chi^2} + \frac{\partial^2\Phi}{\partial\psi^2} = 0 \quad (-\pi/2 < \chi < \pi/2,\ \ 0 < \psi < \psi_0), \tag{6}$$

where the zero flow condition (3) at the rectangular wall is written as

$$\left.\frac{\partial\Phi}{\partial\psi}\right|_{\psi=\psi_0} = 0, \quad \left.\frac{\partial\Phi}{\partial\chi}\right|_{\chi=\pm\pi/2} = 0, \tag{7}$$

and the free surface condition (2) is reformulated as

$$\left[\lambda\gamma(\chi)\Phi + \frac{\partial\Phi}{\partial\psi}\right]_{\psi=0} = 0, \tag{8}$$

where

$$\gamma(\chi) = c\frac{K_2}{K_1}\cos\left(\frac{\pi}{2K_1}\mathrm{sn}^{-1}[\sigma S(\chi)|m_1]\right)\frac{\sigma C(\chi)D(\chi)}{\sqrt{[1-\sigma^2S^2(\chi)][1-m_1\sigma^2S^2(\chi)]}}, \tag{9}$$

in which

$$\begin{aligned}
\sigma &= \mathrm{sn}[(2K_1/\pi)\sin^{-1}[(a-L)/c]|m_1],\\
S(\chi) &= \mathrm{sn}[(2K_2/\pi)\chi|m_2],\\
C(\chi) &= \mathrm{cn}[(2K_2/\pi)\chi|m_2],\\
D(\chi) &= \mathrm{dn}[(2K_2/\pi)\chi|m_2],
\end{aligned} \tag{10}$$

where $\mathrm{cn}[\eta|m] = \cos\varphi$ and $\mathrm{dn}[\eta|m] = \sqrt{1 - m\sin^2\varphi}$ are the Jacobi cosine and Jacobi delta amplitude elliptic functions [29,30].

The possible modes of oscillation are either symmetric or antisymmetric about ψ-axis, which is equivalent to the oscillations being symmetric or antisymmetric about the y-axis (Fig. 2a). For antisymmetric oscillations, the general solution of Eq. (6) satisfying the boundary condition (7) may be obtained by the standard method

of separation of variables as

$$\Phi_A(\chi,\psi)=\sum_{m=1}^{\infty}A_m\frac{\cosh((2m-1)(\psi-\psi_0))}{\cosh((2m-1)\psi_0)}\sin((2m-1)\chi). \tag{11}$$

Substituting the above solution into the free-surface condition (8), making use of the orthogonality property of transcendental functions, and truncating the resulting eigen-system, gives

$$\lambda\sum_{m=1}^{N}A_mI_{nm}^{A}-(2n-1)A_n\tanh((2n-1)\psi_0)=0, \tag{12}$$

where N is the truncation size, $n=1,2,3,\ldots,N$, and $I_{nm}^{A}=(2/\pi)\int_{-\pi/2}^{\pi/2}\gamma(\chi)\sin((2n-1)\chi)\sin((2m-1))\,\mathrm{d}\chi$. Similarly, for symmetric oscillations, the appropriate form of the solution of (6) satisfying (7) is written as

$$\Phi_S(\chi,\psi)=B_0+\sum_{m=1}^{\infty}B_m\frac{\cosh(2m(\psi-\psi_0))}{\cosh(2m\psi_0)}\cos(2m\chi). \tag{13}$$

Incorporating the above solution into the free-surface condition (8), and making use of the orthogonality property of transcendental functions, yields the truncated linear system

$$\lambda\left(B_0+\sum_{m=1}^{N}B_mI_{nm}^{S}\right)-2nB_n\tanh(2n\psi_0)=0, \tag{14}$$

where $n=1,2,3,\ldots,N$, and $I_{nm}^{S}=(2/\pi)\int_{-\pi/2}^{\pi/2}\gamma(\chi)\cos(2n\chi)\cos(2m\chi)\,\mathrm{d}\chi$. Here, we see that the sloshing problem in the baffled elliptic container has been reduced to determining the eigen-values λ for which Eqs. (12) and (14) have non-trivial solutions. The symmetry of the integrals $I_{nm}^{A,S}$ ensures that the associated truncated matrix eigensystem will be symmetric, and thus all eigenvalues are real.

2.2. Unbaffled container

The unbaffled tank geometry is shown in Fig. 1b. Here, the x axis is in the plane of free surface, which occupies $-a<x<a$, and y axis points vertically downwards through the midpoint of the free surface. The successive transformations shown in the second column of Fig. 2 map the inner region of the half-ellipse, shown Fig. 2f, into a strip-like region in Fig. 2i. Such mapping can be constructed in three steps, as explained next. The first two steps are exactly the same as in the case of the baffled container, while the third step involves the function $\xi=2\tanh^{-1}(m_1^{1/4}v)$ which maps the half-disk R_v to a strip like region R_ξ (see Figs. 2f–i) [17]. Consequently, the overall half-ellipse to infinite strip mapping can be written as

$$\xi=\alpha+i\beta=2\tanh^{-1}(m_1^{1/4}\mathrm{sn}[(2K_1/\pi)\sin^{-1}(z/c)|m_1]). \tag{15}$$

A simple comparison of Fig. 2f and i indicates that the intersections of the elliptic container wall with liquid free surface (i.e., points A and A') are now located at $\pm\infty$, and the y-axis coincides with the β-axis. The elliptical container wall coincides with the coordinate line $\beta=\beta_0$ and the liquid free surface coincides with the α-axis.

Next, utilizing the transformation (15), Laplace's equation (1) for the potential $\Phi(\alpha,\beta)$ within R_ξ may be written as

$$\frac{\partial^2\Phi}{\partial\alpha^2}+\frac{\partial^2\Phi}{\partial\beta^2}=0\quad(-\infty<\alpha<\infty,\ \ 0<\beta<\beta_0), \tag{16}$$

where the zero flow condition (3) at the upper boundary of the strip is written as

$$\left.\frac{\partial\Phi}{\partial\beta}\right|_{\beta=\beta_0}=0, \tag{17}$$

and the free surface condition (2) is reformulated as

$$\left[\lambda\gamma(\alpha)\Phi+\frac{\partial\Phi}{\partial\beta}\right]_{\beta=0}=0, \tag{18}$$

where

$$\gamma(\alpha)=\frac{c\pi}{4m_1^{1/4}K_1}\frac{\cos((\pi/2K_1)\mathrm{sn}^{-1}[m_1^{-1/4}\tanh(\alpha/2)|m_1])[1-\tanh^2(\alpha/2)]}{\sqrt{[1-m_1^{-1/2}\tanh^2(\alpha/2)][1-m_1^{1/2}\tanh^2(\alpha/2)]}}. \tag{19}$$

For antisymmetric and symmetric oscillations, the general solution of (16) satisfying the boundary condition (17) may, respectively, be stated in terms of the appropriate Fourier integrals as

$$\Phi_A(\alpha,\beta)=\int_0^\infty A(\overline{\tau})\frac{\cosh[\overline{\tau}(\beta-\beta_0)]}{\cosh(\overline{\tau}\beta_0)}\sin(\overline{\tau}\alpha)\,\mathrm{d}\overline{\tau}$$

$$\Phi_S(\alpha,\beta)=\int_0^\infty B(\overline{\tau})\frac{\cosh[\overline{\tau}(\beta-\beta_0)]}{\cosh(\overline{\tau}\beta_0)}\cos(\overline{\tau}\alpha)\,\mathrm{d}\overline{\tau}. \tag{20}$$

Substituting the above solution into the free-surface condition (18) and making further use of the Fourier sine and cosine transformations, yields the corresponding integral eigen-value problems

$$\lambda\int_0^\infty A(\overline{\tau})I_A(\tau,\overline{\tau})\mathrm{d}\overline{\tau}-\tau\tanh(\tau\beta_0)A(\tau)=0$$

$$\lambda\int_0^\infty B(\overline{\tau})I_S(\tau,\overline{\tau})\mathrm{d}\overline{\tau}-\tau\tanh(\tau\beta_0)B(\tau)=0, \tag{21}$$

where

$$I_A(\tau,\overline{\tau})=\frac{2}{\pi}\int_0^\infty\gamma(\alpha)\sin(\tau\alpha)\sin(\overline{\tau}\alpha)\,\mathrm{d}\alpha$$

$$I_S(\tau,\overline{\tau})=\frac{2}{\pi}\int_0^\infty\gamma(\alpha)\cos(\tau\alpha)\cos(\overline{\tau}\alpha)\,\mathrm{d}\alpha. \tag{22}$$

The above integral eigen-value problems can readily be converted into symmetric matrix eigen-value problems with real eigen-values using the $\overline{N}$-point Gauss–Laguerre quadrature formula in the form [29]

$$\int_0^\infty g(\tau,\overline{\tau})\,\mathrm{d}\overline{\tau}\approx\sum_{i=1}^{\overline{N}}w_i\exp(\tau_i)g(\tau,\tau_i), \tag{23}$$

where $\overline{\tau}_i$ are the abscissas, w_i $(i=1,2,\ldots,\overline{N})$ are the weighting coefficients, and $g(\tau,\overline{\tau})$ can be either $A(\overline{\tau})I_A(\tau,\overline{\tau})$ or $B(\overline{\tau})I_S(\tau,\overline{\tau})$. Using the above formula to treat the integral equations (21) in this way, after some manipulations, leads to the standard matrix eigen-problems

$$\lambda\mathbf{M}_A\mathbf{A}=\mathbf{K}\mathbf{A}$$

$$\lambda\mathbf{M}_S\mathbf{B}=\mathbf{K}\mathbf{B}, \tag{24}$$

where the elements of the vector $\mathbf{A}=[A_j=A(\tau_j)]$, $\mathbf{B}=[B_j=B(\tau_j)]$ $(j=1,2,\ldots,\overline{N})$, are unknown Fourier coefficients, $\mathbf{K}=[K_{ij}]=\mathrm{Diag}[\tau_i\tanh\tau_i\beta_0](i,j=1,2,\ldots,\overline{N})$, and the elements of the square matrices $\mathbf{M}_A=[M_{ij}^A]$ and $\mathbf{M}_S=[M_{ij}^S]$ are given as

$$M_{ij}^{A,S}=w_i\exp(\tau_i)I_{A,S}(\tau_j,\tau_i), \tag{25}$$

where the kernel integrals $I_A(\tau_i,\tau_j,m)$ and $I_S(\tau_i,\tau_j,m)$ may readily be evaluated using standard numerical integration routines. This completes the necessary background required for the analysis of the problem. Next we consider detailed numerical examples.

3. Numerical results

In this section, noting the relatively straightforward computations involved here, a detailed parametric study is carried out to investigate the effects of the key geometric parameters, namely the container aspect

ratio a/b and the baffle extension ratio L/a, on the natural sloshing frequencies. From the collection of data presented here, certain trends are noted and general conclusions are made about the relative importance of the parameters. A Mathematica code was developed for computation of the eigen-values from the eigen-systems (12), (14) and (24) based on the standard bisection root finding technique. The numerical integrations in $I_{nm}^{A,S}$ and $I_{A,S}$ are performed by making extensive use of the Mathematica build-in function "NIntegrate [31]." The convergence of numerical calculations were ensured by increasing the truncation size (for the baffled container) or discretization order (for the unbaffled vessel), while looking for steadiness in the numerical value of the computed natural frequencies.

3.1. Convergence and computation time

The first column in Fig. 3 shows the change in the first three normalized antisymmetric and symmetric sloshing frequencies ($\Omega = \omega^2\sqrt{ab}/g$) with the truncation size, N, for four selected container geometries for the

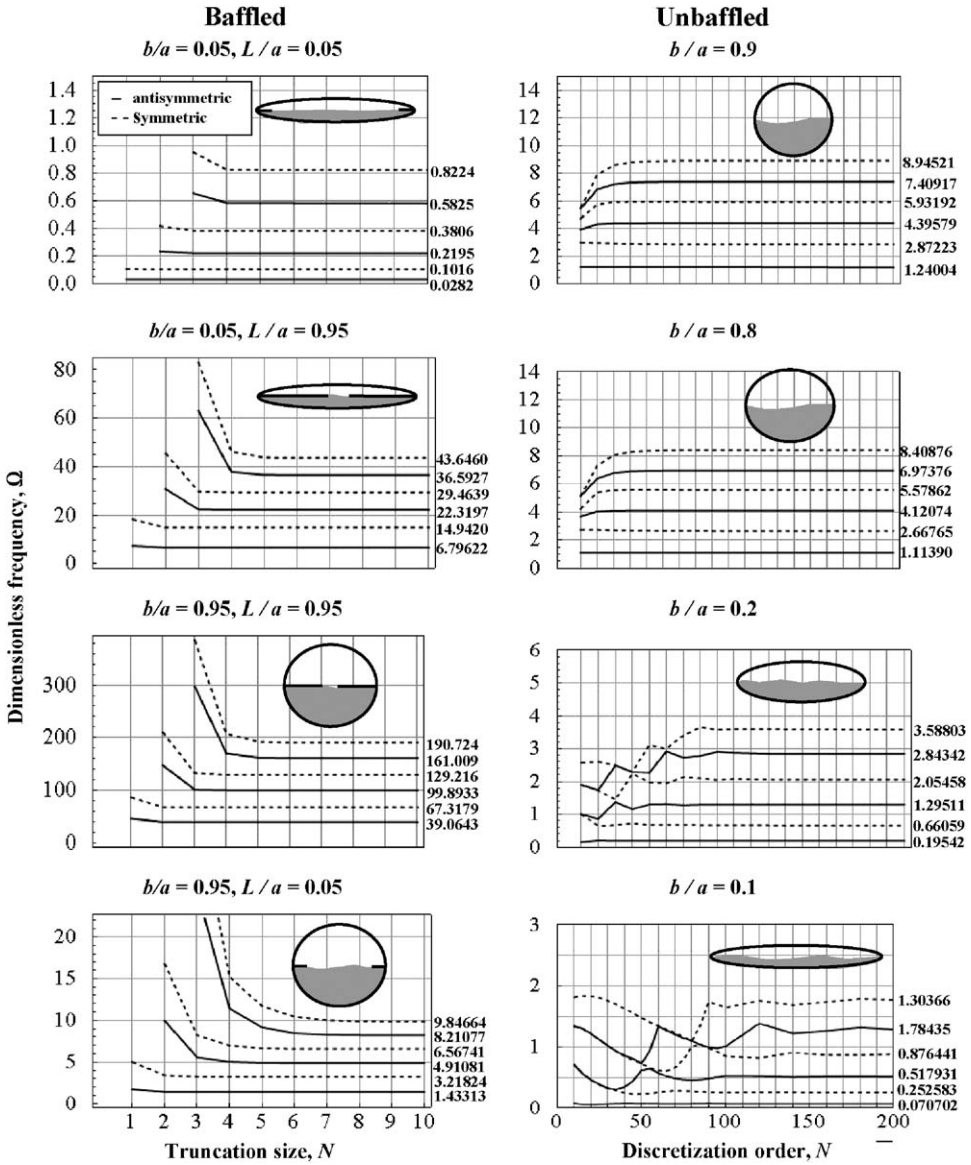

Fig. 3. The change in the first three normalized antisymmetric and symmetric sloshing frequencies ($\Omega = \omega^2\sqrt{ab}/g$) with the truncation size (discretization order) for four selected container geometries for the baffled (unbaffled) vessel.

Table 1
Comparison of the total CPU times for calculating the sloshing frequencies for nearly-circular and highly-elliptical tanks of extremely short baffles with their unbaffled counterparts.

	Baffled tank ($L/a = 0.0001$)			Unbaffled tank		
	A	S	CPU time (s)	A	S	CPU time (s)
$b/a = 0.1$	0.070710	0.246522	338	0.070702	0.252583	124,308
	0.517798	0.872455		0.517931	0.876441	
	1.29632	1.77456		1.30366	1.78435	
$b/a = 0.9$	1.24030	2.8475	2,685	1.24004	2.87223	30,854
	4.39672	5.90922		4.39579	5.93192	
	7.41178	8.90958		7.40917	8.94521	

baffled vessel ($L/a, b/a = 0.05, 0.95$). It is clear that the fastest convergence is obtained for the container with the highest aspect ratio and shortest baffle (i.e., for $b/a = L/a = 0.05$). This may be explained by the fact that the modal oscillations in the fluid-layer-like container can more suitably be described by the adopted transcendental series type solutions (11) and (13). Consequently, as the container shape departs from a nearly-rectangular shaped region (e.g., for the circular container), the liquid sloshing modes are expected to get more coupled and deviate from the sinusoidal form. Thus, more terms in the series solution are rationally needed for obtaining accurate solutions. In addition, the frequency convergence plots for the elliptic and the nearly-circular containers with long baffle extensions (i.e., for $b/a = 0.05, 0.95$; $L/a = 0.95$) display a similar trend. This implies that for a narrow free surface length, the natural frequencies are expected to be nearly insensitive with respect to the overall container geometry. Lastly, one can note that, even in the worst situation (e.g., for the third symmetric mode in a nearly-circular tank with very short baffles), no more than 10 terms are needed in the series to obtain an acceptable accuracy ($N < 10$). The second column in Fig. 3 shows the change in the first three normalized antisymmetric and symmetric sloshing frequencies($\Omega = \omega^2\sqrt{ab}/g$), obtained by the $\overline{N}$-point Gauss–Laguerre quadrature formula, with the discretization order for four selected geometric ratios of the unbaffled vessel ($b/a = 0.1, 0.2, 0.8, 0.9$). A distinctively different trend, in comparison with the baffled container is observed. In particular, in contrast with the Fourier series solution obtained for the baffled container, the fastest (slowest) convergence is obviously observed for the container with the lowest (highest) aspect ratio, i.e., for $b/a = 0.9$ ($b/a = 0.1$).

Table 1, compares the total CPU times spent on a low-end personal computer for calculating the first three antisymmetric and symmetric sloshing frequencies for nearly-circular and highly elliptical tanks of extremely short baffles ($b/a = 0.1, 0.9$; $L/a = 0.0001$) with those of unbaffled tanks of identical geometric ratios ($b/a = 0.1, 0.9$). While an acceptable agreement in the natural frequencies is observed, the computation times for the baffled containers are obviously lower than those of the unbaffled vessels. This is mainly because of the (earlier-noted) fast convergence of Fourier series solution (in addition to the lower computation time required for evaluating the proper integrals $I_{nm}^{A,S}$) for the baffled container, in comparison with the lower rate of convergence obtained by using the $\overline{N}$-point Gauss–Laguerre quadrature approximation formula (along with the higher computation time needed for evaluating the improper integrals $I_{A,S}$; see Eqs. (22)) in the unbaffled case. In particular, we note for the baffled (unbaffled) vessel that, the computation time for a highly elliptic cross section is markedly lower (higher) than that of a nearly-circular section. Moreover, the total CPU time for the highly elliptic vessel with very short side baffles ($b/a = 0.1$; $L/a = 0.0001$) is stunningly lower than that of the unbaffled elliptic vessel ($b/a = 0.1$). Therefore, it is reasonable to conclude that the total computation time for calculation of the natural sloshing frequencies of highly elliptic half-full unbaffled containers with acceptable accuracy may appreciably be reduced by employing the Fourier series approach, while assuming the presence of a pair of very small side-baffles.

3.2. Numerical examples

Fig. 4 displays the 2D contour plots of first three antisymmetric and symmetric dimensionless sloshing frequencies ($\Omega = \omega^2 b/g$) as a function of the geometric ratio, b/a, and baffle extension ratio, L/a, for vessels of

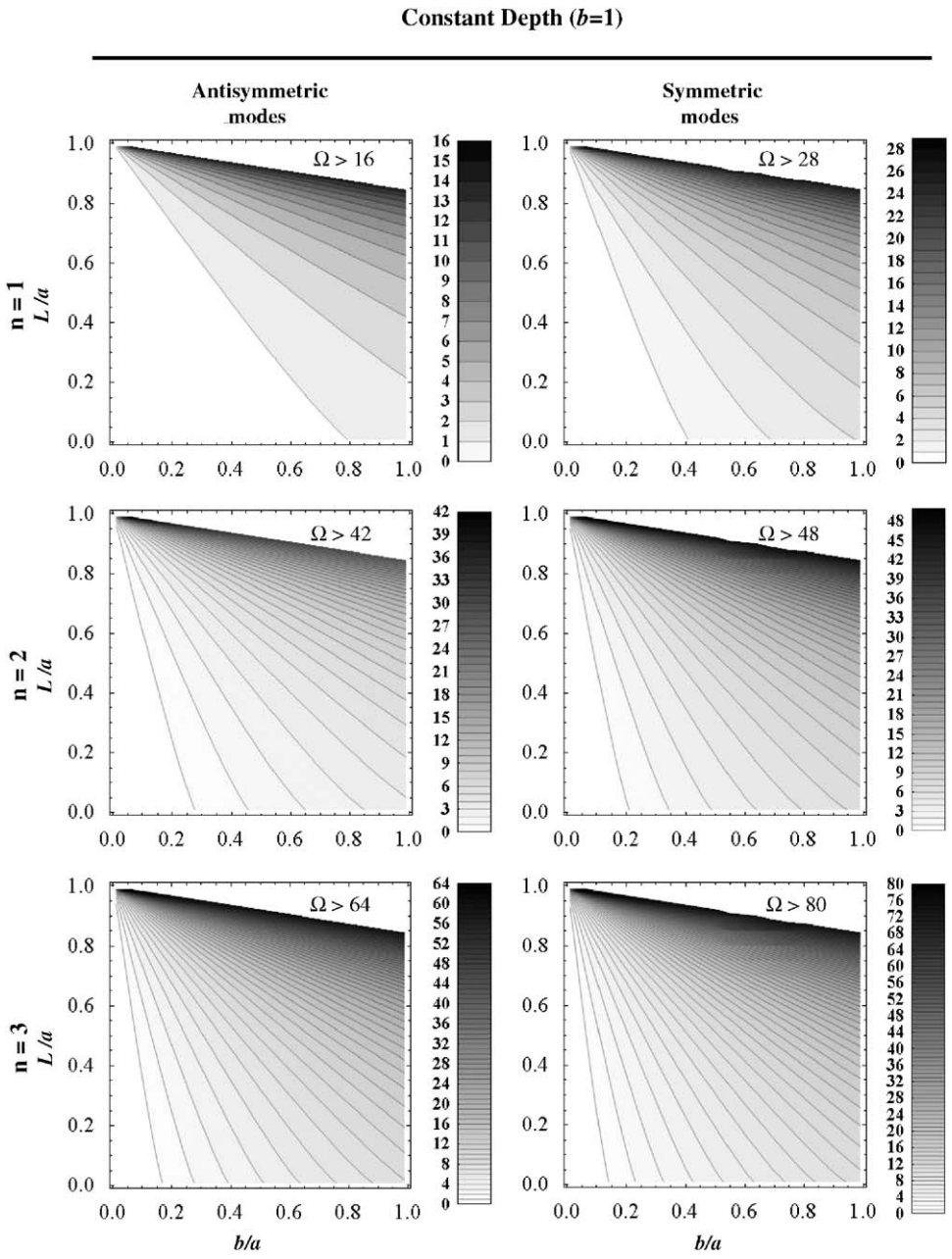

Fig. 4. The 2D contour plots of first three antisymmetric and symmetric dimensionless sloshing frequencies ($\Omega = \omega^2 b/g$) as functions of the container geometric and baffle extension ratios for vessels of constant depth.

constant depth (i.e., $b = 1$). The most important observations are as follows. The natural frequencies increase with increasing b/a and also with L/a. In particular, for a fixed baffle length ratio, the sloshing frequencies increase from zero to a finite value as the as b/a increases from zero to unity (i.e., by moving from a film-like geometry towards a circular one). This increase in the natural frequencies may naturally be linked to the decrease in the free surface width (relative to the container depth) as b/a increases. Also, for a fixed tank geometric ratio, the sloshing frequencies increase from a finite value to infinity as the as L/a increases from zero to unity. This remarkable increase in the natural frequencies may directly be linked to the vanishing of the free surface width as L/a approaches unity. Here, we note that in order to get a better presentation of the

results, the extremely high values of natural frequency obtained in the vicinity of the $L/a = 1$ line have not been displayed in the subplots. Furthermore, it is clear that the constant frequency contour lines for the constant depth vessel appear to be nearly straight lines which originate from the point $(b/a, L/a) = (0, 1)$. This implies that, regardless of container's width or aspect ratio, all vessels of constant depth (b) and equal free surface length ($a-L$) are expected to share nearly equal sloshing frequencies. Additionally, the slope, $-(a-L)/b$, of the constant frequency lines decrease as either L/a or b/a increases. In particular, when the slope of the constant frequency line is high, the sensitivity of natural frequencies with respect to the geometric ratio, b/a, is high in comparison with that of the baffle extension ratio, L/a. On the other hand, when the slope of the constant frequency line is low, the natural frequencies do not display a great sensitivity with respect to the change in the geometric ratio, b/a, in comparison with that of the baffle extension ratio, L/a. In other words, when there is a wide liquid free surface length relative to the container depth, the natural frequencies will be very sensitive with respect to the geometric container aspect ratio. Conversely, for a narrow free surface length, the natural frequencies are nearly insensitive with respect to the container geometry. This may be because, changing the b/a ratio in the latter case does not change the active oscillating liquid mass in the vicinity of the free surface. Lastly, one can note that the compactness of the constant frequency lines (or rate of increase in the frequency magnitudes) increases, as the free surface length decreases (i.e., either L/a or b/a increases).

Fig. 5 shows the 2D contour plots of first three normalized antisymmetric and symmetric sloshing frequencies ($\Omega = \omega^2 a/g$) as a function of the tank aspect ratio and baffle extension ratio for vessels of constant width (i.e., $a = 1$). Comments very similar to above remarks can readily be made. The most important distinction is that the sensitivity of natural frequencies with respect to the change in the geometric ratio, b/a, is rapidly lost, especially for higher mode numbers and/or high baffle extension ratios, L/a. In particular, there exists a critical container aspect ratio (or equivalently a critical container depth), for which the natural frequencies start to loose their sensitivities. This implies that, for each given liquid free surface length (or L/a), there is a specific (critical) container depth before which increasing container depth (i.e., adding active oscillating liquid mass) affects the natural liquid sloshing frequencies. On the other hand, as the container depth is increased beyond the critical value (i.e., adding inactive liquid mass), the constant frequency contour lines become nearly horizontal, and the sloshing frequencies do not exhibit any notable change with the geometric ratio, b/a. Further examination of the figure indicates that, the numerical value of the critical container geometric ratio decreases with increasing the mode number. This can be explained by the fact that liquid oscillations in higher modes is actively confined in the vicinity of free surface. In addition, the critical geometric ratio for containers with long baffles (i.e., a narrow liquid free surface) appear to be smaller than those with short baffles (i.e., a wide liquid free surface). This may be because, in contrast with the wide free surface case, a narrow free surface length is not capable of actively setting a great amount of liquid mass in oscillations.

Fig. 6 displays the 2D contour plots of first three normalized antisymmetric and symmetric sloshing frequencies ($\Omega = \omega^2\sqrt{ab}/g$) as a function of the tank aspect ratio and baffle extension ratio for vessels of constant capacity (i.e., $\sqrt{ab} = 1$), which may be of most practical value for design and optimization purposes [26]. Comments very similar to those made in the previous two figures can be made. The most important differences are that here the constant frequency contour lines are not linear (as in Fig. 4), and there is no distinct critical container depth for frequency insensitivity with respect to the container aspect ratio (as in Fig. 5). In other words, the sloshing frequency contours for the constant capacity container behave somewhat in between those for the constant depth and the constant width vessels.

A more detailed presentation of the numerical results may be obtained by slicing the contour plots in Figs. 4–6 along the constant baffle extension ratio lines. Accordingly, the three columns displayed in Fig. 7 show the variation in the first three normalized antisymmetric and symmetric sloshing frequencies with the cross sectional aspect ratio for constant depth, width, and capacity tanks of selected baffle extension ratio ($L/a = 0.01, 0.1, \ldots, 0.90, 0.95$). Here, nearly all above-mentioned observations are more clearly illustrated (i.e., the linear frequency dependence for constant depth vessel, and the distinct critical depth for the constant width vessel). The most interesting observation is perhaps that the initial slope of the frequency—b/a curves (i.e., the slope at $b/a \approx 0$) increases from near zero to infinity, as the baffle extension ratio (L/a) increases. This effect, which is most clearly observable for the constant capacity vessel (i.e., in the last column of Fig. 7), may be explained as described earlier in discussions of Figs. 4–6.

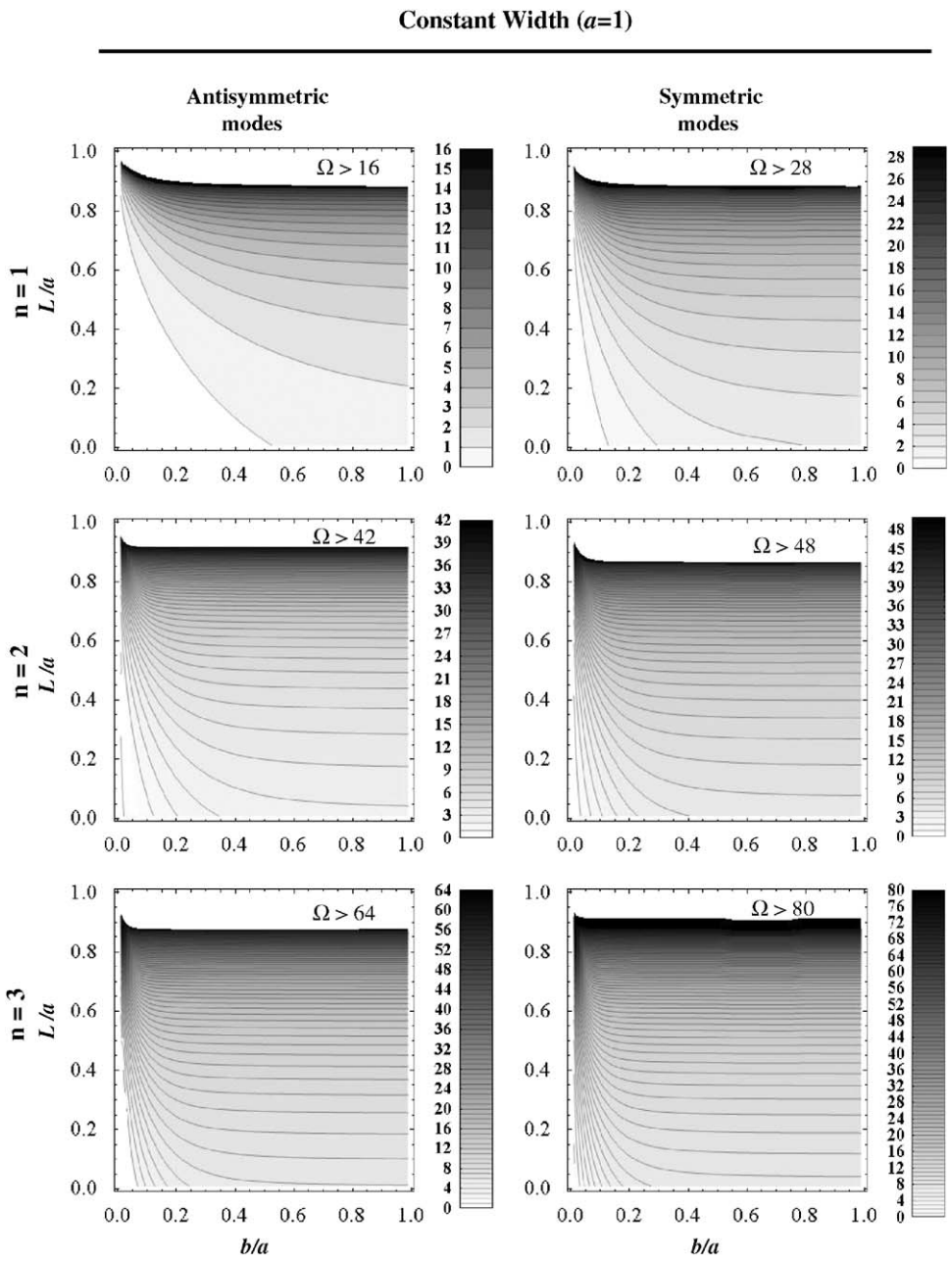

Fig. 5. The 2D contour plots of first three antisymmetric and symmetric dimensionless sloshing frequencies ($\Omega = \omega^2 a/g$) as functions of the container geometric and baffle extension ratios for vessels of constant width.

3.3. Computer code validation

Finally, in order to show overall validity of the solutions, we used our general Mathematica codes to compute the first three normalized antisymmetric and symmetric sloshing frequencies ($\Omega = \omega^2\sqrt{ab}/g$) for a wide range of aspect ratios and baffle lengths of a constant capacity vessel (i.e., $\sqrt{ab} = 1$), with the aim of matching the theoretical [16,20], numerical [28], and experimental [1] results available in the open literature. The outcome is displayed in Table 2. The calculated natural frequencies, which are predominantly validated to at least three decimal digits, along with the related references are tabulated. It should be reminded that the

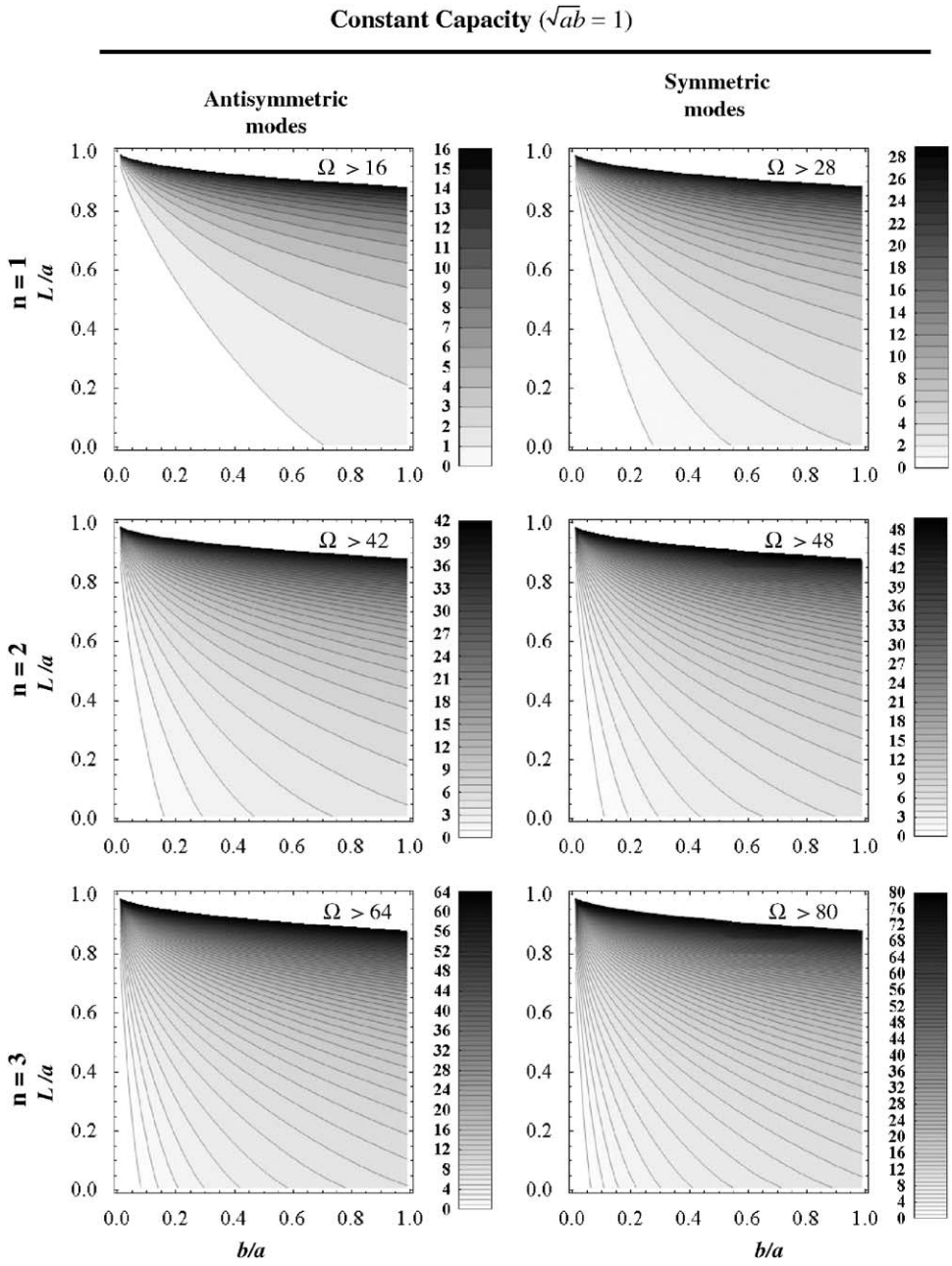

Fig. 6. The 2D contour plots of first three antisymmetric and symmetric dimensionless sloshing frequencies ($\Omega=\omega^2\sqrt{ab}/g$) as functions of the container geometric and baffle extension ratios for vessels of constant capacity.

numerical values of the natural frequencies listed in Table 2 are normalized with respect to characteristic length $\sqrt{ab}$. Therefore, proper scaling in each case must separately be performed in order to obtain the specific values presented in the above-mentioned references.

4. Conclusions

A simple and computationally efficient semi-analytic approach based on the linearized theory of water waves in conjunction with the powerful conformal mapping technique is employed to investigate free lateral

(2D) sloshing inside a half-full horizontal elliptical vessel without or with a pair of longitudinal side baffles of arbitrary extension. In particular, a detailed parametric study for examining the influence of the container's cross sectional ellipticity and the side-baffle lengths on the calculated liquid natural frequencies is performed. The most important observations are summarized as follows.

The fastest convergence (smallest CPU time) is obtained via Fourier series in the calculation of natural frequencies for the container with the highest aspect ratio and shortest side baffles. Also, the convergence rate for the baffled vessel with a very narrow free liquid surface (or long baffles) is found to be nearly insensitive with respect to the overall tank geometry. On the other hand, the slowest convergence (highest CPU time) in the calculation of natural frequencies is observed when using Gauss–Laguerre quadrature technique for the

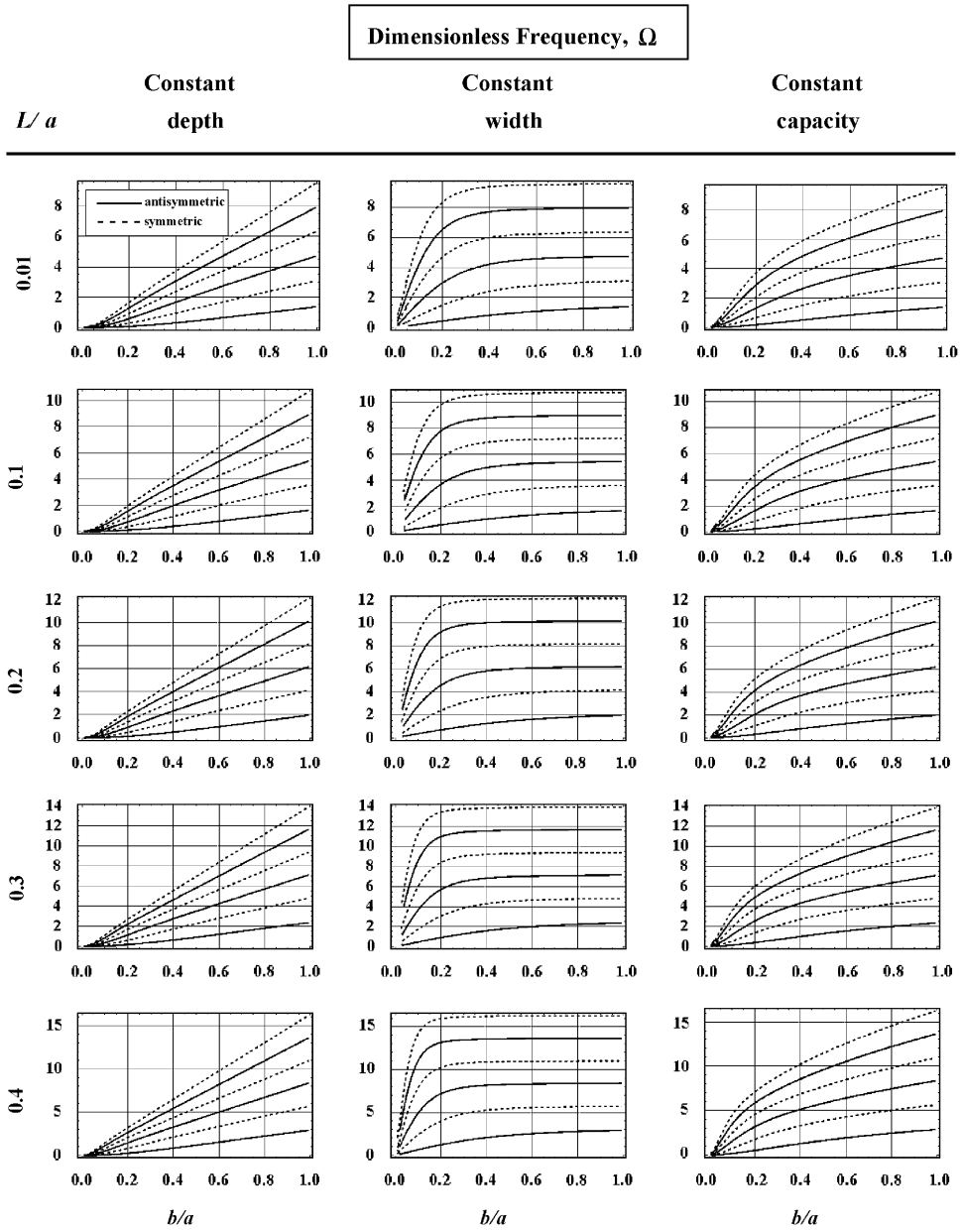

Fig. 7. The variation in the first three normalized antisymmetric and symmetric sloshing frequencies with the cross sectional aspect ratio for constant depth, constant width, and constant capacity tanks of selected baffle extension ratios.

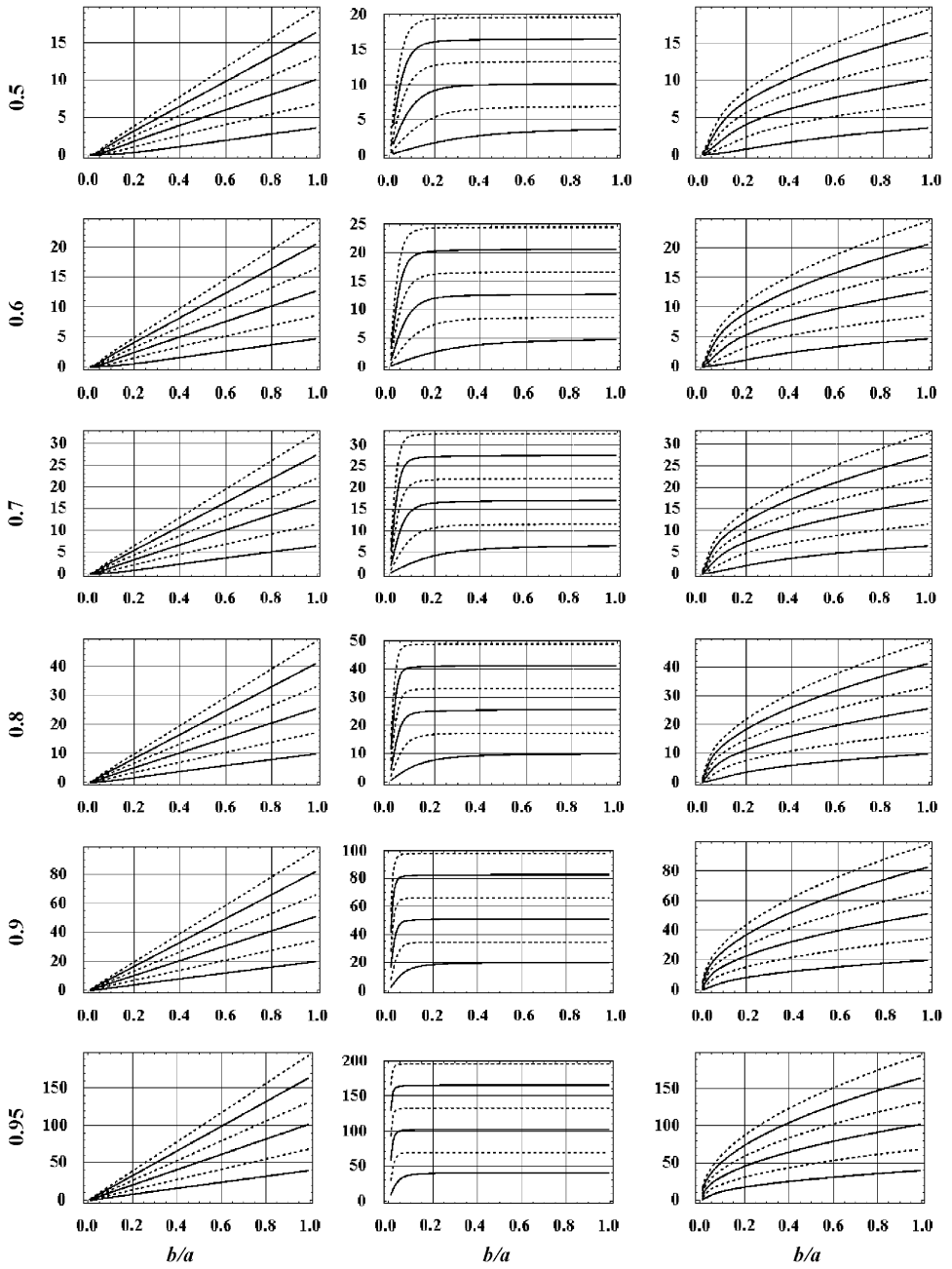

Fig. 7. (*Continued*)

highly elliptical unbaffled vessel. In particular, it is demonstrated that the Fourier series approach for a highly elliptical (nearly circular) container with a pair of very short side-baffles may advantageously be used to enormously (considerably) reduce the total computation time for calculation of the natural sloshing frequencies of the unbaffled container with an acceptable accuracy.

It is found that the natural sloshing frequencies generally increase with decreasing tank aspect ratio and/or increasing the side baffle lengths. In particular, the effect of increasing the baffle lengths on boosting the natural sloshing frequencies is more prominent for the nearly circular container in comparison with that of the highly elliptical container. Furthermore, all elliptical vessels of constant depth and equal free liquid surface

Table 2
The first three normalized antisymmetric and symmetric sloshing frequencies for a wide range of (constant capacity) tank aspect ratios and baffle lengths.

b/a	n	$L/a = 0.0001$		$L/a = 0.1$		$L/a = 0.5$		$L/a = 0.9$	
		A	S	A	S	A	S	A	S
0.4359	1	0.5671	1.6261	0.7030 [16]	1.9956 [16]	1.9070	4.3794	13.0156	22.7975
	2	2.7944	3.9319	3.3384 [16]	4.6074 [16]	6.5795	8.6974	33.7691	43.7632
	3	5.0290	6.1018	5.8262 [16]	7.0197 [16]	10.8017	12.8871	54.4947	64.5960
0.5000	1	0.6713 [28]	1.8471 [28]	0.8289	2.2472	2.1674	4.7502	13.9959	24.4173
	2	3.0876 [28]	4.2802 [28]	3.6583	4.9882	7.0772	9.3308	36.1835	46.8710
	3	5.4356 [28]	6.5723	6.2762	7.5445	11.5837	13.8110	58.3737	69.1829
0.7285	1	1.0171 [1]	2.4813	1.2413	2.9604	2.9414	5.8351	17.0081	29.4745
	2	3.9092	5.2866	4.5674	6.1151	8.6139	11.2924	43.7102	56.5767
	3	6.6463	7.9984	7.6411	9.1559	14.0216	16.6878	70.4806	83.5084
0.8000	1	1.1141 [28]	2.6426 [28]	1.3558	3.1416	3.1445	6.1271	17.8412	30.8872
	2	4.1216 [28]	5.5560 [28]	4.8070	6.4212	9.04055	11.8376	45.8106	59.2882
	3	6.9765 [28]	8.3910	8.0169	9.6021	14.7016	17.4899	73.8615	87.5106
0.8660	1	1.1986	8.7368	1.4552	3.2967	3.3193 [16]	6.3830 [16]	18.5758	32.1361
	2	4.3057	5.7918	5.0159	6.6901	9.4169 [16]	12.319 [16]	47.6669	61.6854
	3	7.2669	2.7802	8.3480	9.9956	15.302 [16]	18.1987 [16]	76.8503	91.0489
0.9950	1	1.3505	3.0248	1.6334	3.57361	3.6320	6.8527	19.9309 [16]	34.4467 [16]
	2	4.6396	6.2243	5.3974	7.18448	10.1114	13.2085	51.0999 [16]	66.1204 [16]
	3	7.8015	9.3747	8.9587	10.7221	16.4125	19.5094	82.3790 [16]	97.5950 [16]
0.9999	1	1.3559 [20]	3.0336 [20]	1.6398	3.5836	3.6432	6.8699	19.9805	34.5314
	2	4.6517 [20]	6.2401 [20]	5.4113	7.2025	10.1368	13.2411	51.2258	66.2830
	3	7.8210 [20]	9.3981 [20]	8.9811	10.7487	16.4532	19.5574	82.5817	97.8350

length appear to share nearly the same sloshing frequencies, regardless of their aspect ratio or baffle extension. Also, when the free liquid surface is wide (narrow) relative to the container depth, the natural frequencies are found to be very sensitive (nearly insensitive) with respect to the container cross sectional ellipticity. When the width of the container is kept constant, for each given free liquid surface length, there is a critical container geometric ratio after which the natural frequencies remain practically unaffected. This critical value decreases with increasing the mode number and/or baffle extension. For containers of constant capacity, there is no distinct critical aspect ratio observed, and the natural frequencies exhibit a general behavior which is somewhat in between those of the constant depth and the constant width vessels.

Acknowledgments

The authors wish to thank professors J.A. Romero, S. Rakheja, C.M. Linton, and W. Eidel for providing the authors with copies of their valuable works.

References

[1] J.A. Romero, R. Hildebrand, M. Martínez, O. Ramírez, J.M. Fortanell, Natural sloshing frequencies of liquid cargo in road tankers, *International Journal of Heavy Vehicle Systems* 12 (2005) 121–138.
[2] H.F. Bauer, Fluid oscillations in the containers of a space vehicle and their influence upon stability, NASA-TR-R-187, 1964.

[3] R.A. Ibrahim, *Liquid Sloshing Dynamics*, Cambridge University Press, Cambridge, 2005.
[4] H.F. Bauer, Oscillations of non-viscous liquid in various container geometries Forschungsbericht LRT-WE-9-FB-1, 1999.
[5] W. Wei, L. Junfeng, W. Tianshu, Modal analysis of liquid sloshing with different contact line boundary conditions using FEM, *Journal of Sound and Vibration* 317 (2008) 739–759.
[6] D. Liu, P. Lin, A numerical study of three-dimensional liquid sloshing in tanks, *Journal of Computational Physics* 227 (2008) 3921–3939.
[7] S. Mitra, P.P. Upadhyay, K.P. Sinhamahapatra, Slosh dynamics of inviscid fluids in two dimensional tanks of various geometry using finite element method, *International Journal of Numerical Methods in Fluids* 56 (2008) 1625–1651.
[8] J.C. Viralla, C.A. Prato, L.A. Godoy, Linear and nonlinear 2D finite element analysis of sloshing modes and pressures in rectangular tanks subject to horizontal harmonic motions, *Journal of Sound and Vibration* 312 (2008) 442–460.
[9] A. Maleki, M. Ziyaeifar, Sloshing damping in cylindrical liquid storage tanks with baffles, *Journal of Sound and Vibration* 311 (2008) 372–385.
[10] G.C. Drosos, A.A. Dimas, D.L. Karabalis, Discrete models for seismic analysis of liquid storage tanks of arbitrary shape and fill height, *Journal of Pressure Vessel Technology* 130 (2008) 0418011–04180112.
[11] N.K.A. Attari, F.R. Rofooei, On lateral response of structures containing a cylindrical liquid tank under the effect of fluid/structure resonances, *Journal of Sound and Vibration* 318 (2008) 1154–1179.
[12] B. Budiansky, Sloshing of liquids in circular canals and spherical tanks, *Journal of Aerospace Sciences* 27 (1960) 161–173.
[13] J.L. McCarty, D. Stephens, Investigation of the natural frequencies of fluids in spherical and cylindrical tanks, NASA-TN-D-252, 1960.
[14] D.D. Kana, Liquid slosh response in horizontal cylindrical tank under seismic excitation, Rep. No. 02–9238, Southwest Research Institute, San Antonio, Tex., 1979.
[15] N.N. Moiseev, A.A. Petrov, The calculation of free oscillations of a liquid in a motionless container, *Advances in Applied Mechanics* 9 (1966) 91–154.
[16] D.W. Fox, J.R. Kutler, Sloshing frequencies, *Journal of Applied Mathematics and Physics ZAMP* 34 (1983) 669–696.
[17] P. McIver, Sloshing frequencies for cylindrical and spherical containers filled to an arbitrary depth, *Journal of Fluid Mechanics* 201 (1989) 243–257.
[18] N. Kobayashi, T. Mieda, H. Shibata, Y. Shinozaki, A study of the liquid slosh response in horizontal cylindrical tanks, *Journal of Pressure Vessel Technology* 111 (1989) 32–38.
[19] P. McIver, M. McIver, Sloshing frequencies of longitudinal modes for a liquid contained in a trough, *Journal of Fluid Mechanics* 252 (1993) 525–541.
[20] D.V. Evans, C.M. Linton, Sloshing frequencies, *Quarterly Journal of Mechanics and Applied Mathematics* 46 (1993) 71–87.
[21] S. Papaspyrou, S.A. Karamanos, D. Valougeorgis, Response of half full horizontal cylinders under transverse excitation, *Journal of Fluids and Structures* 19 (2004) 985–1003.
[22] S. Papaspyrou, D. Valougeorgis, S.A. Karamanos, Sloshing effects in half-full horizontal cylindrical vessels under longitudinal excitation, *ASME Journal of Applied Mechanics* 71 (2004) 255–265.
[23] L. Patkas, S.A. Karamanos, Variational solutions of externally-induced sloshing in horizontal-cylindrical and spherical vessels, *ASCE Journal of Engineering Mechanics* 133 (2007) 641–655.
[24] L. Strandberg, Lateral stability of road tankers, VTI Report No. 138A, Sweden, Vol. 1, 1978.
[25] S. Rakheja, S. Sankar, R. Ranganathan, Influence of tank design factors on the rollover threshold of partially filled tank vehicles. SAE Technical Paper Series, No.892480. Truck and Bus Meeting and Exposition, Charlotte, North Carolina, November 6–9, 1989.
[26] G. Popov, S. Sankar, T.S. Sankar, Shape optimization of elliptical road containers due to liquid load in steady-state turning, *Vehicle System Dynamics* 25 (1996) 203–221.
[27] M. Salem, Rollover Stability of Partially Filled Heavy-duty Elliptical Tankers Using Trammel Pendulums to Simulate Fluid Sloshing, Ph.D. Thesis, West Virginia University, 2000.
[28] L. Xu, Fluid Dynamics in Horizontal Cylindrical Containers and Liquid Cargo Vehicle Dynamics, Ph.D. Thesis, University of Regina, Saskatchewan, 2005.
[29] M. Abramowitz, I.A. Stegun, *Handbook of Mathematical Functions*, National Bureau of Standards, Washington, DC, USA, 1964.
[30] Z. Nehari, *Conformal Mapping*, Dover Publications, New York, 1975.
[31] S. Wolfram, *Mathematica: A System for Doing Mathematics by Computer*, second ed., Addison Wesley Publishing Company, Reading, MA, 1991.